Biomacromolecules

pubs.acs.org/Biomac

Article

Control over Imidazoquinoline Immune Stimulation by pH-Degradable Poly(norbornene) Nanogels

Johannes Kockelmann, Judith Stickdorn, Sabah Kasmi, Jana De Vrieze, Michaela Pieszka, David Yuen W. Ng, Sunil A. David, Bruno G. De Geest, and Lutz Nuhn*

Cite This: *Biomacromolecules* 2020, 21, 2246−2257

Read Online

ACCESS | Metrics & More | Article Recommendations | Supporting Information

ABSTRACT: The reactivation of the innate immune system by toll-like receptor (TLR) agonists holds promise for anticancer immunotherapy. Severe side effects caused by unspecific and systemic activation of the immune system upon intravenous injection prevent the use of small-molecule TLR agonists for such purposes. However, a covalent attachment of small-molecule imidazoquinoline (IMDQ) TLR7/8 agonists to pH-degradable polymeric nanogels could be shown to drastically reduce the systemic inflammation but retain the activity to tumoral tissues and their draining lymph nodes. Here, we introduce the synthesis of poly(norbornene)-based, acid-degradable nanogels for the covalent ligation of IMDQs. While the intact nanogels trigger sufficient TLR7/8 receptor stimulation, their degraded version of soluble, IMDQ-conjugated poly(norbornene) chains hardly activates TLR7/8. This renders their clinical safety profile, as degradation products are obtained, which would not only circumvent nanoparticle accumulation in the body but also provide nonactive, polymer-bound IMDQ species. Their immunologically silent behavior guarantees both spatial and temporal control over immune activity and, thus, holds promise for improved clinical applications.

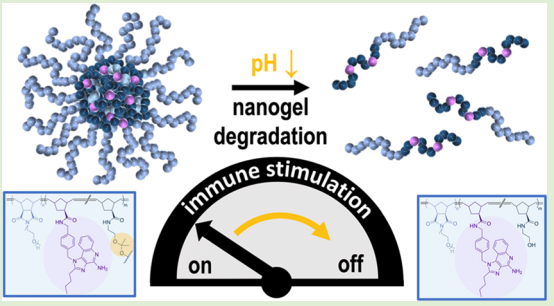

INTRODUCTION

The maturation of dendritic cells (DCs) to antigen-presenting cells, the subsequent development of a T-cell-dependent immune reaction, and the secretion of various chemokines are of key interest in cancer immunotherapy.[1] However, these mechanisms are often disabled in tumoral tissues.[2] On the contrary, immature DCs suppress the activity of self-reactive, anticancer T-cells and support the proliferation of immunosuppressive T-cells.[3,4] Therefore, strong activators of the innate immune system in the tumor microenvironment could enhance DC maturation, lead to the depletion of anti-inflammatory signals, induce the proliferation of antitumoral T-cells, and turn immunologically "cold" tumors into "hot".[5]

A strategy to increase the DC maturation and antigen presentation to T-cells includes the activation of toll-like receptors (TLR).[6] These receptors normally recognize pathogen-associated molecular patterns (PAMPs) like lipopolysaccharides, double- or single-stranded RNA, etc. Their activation leads to the differentiation of immature DCs and the stimulation of an active immune response.[7] Among others, potent TLR agonists like the TLR-7/8 agonist imidazoquinoline (IMDQ) are under investigation as adjuvants in vaccination[8] as well as for their use in anticancer immunotherapy.[9]

Unfortunately, the administration of the immunostimulant IMDQ leads to a systemic activation of the immune system due to the unfavorable pharmacokinetic profile of the small-molecule drug.[10−12] This may even trigger life-threatening inflammatory cascade reactions, e.g., cytokine storms.[13] Alternatively, the conjugation of a small-molecule IMDQ to a nanoparticulate carrier was shown by others and us to improve the pharmacokinetic parameters and constrain the immune activity to the site of interest.[14−20]

The covalent attachment of IMDQ to a poly(methacrylamide)-based nanogel carrier was shown to result in a more defined pharmacological profile in terms of spatial control upon peritumoral injection and accumulation in the draining lymph nodes.[11,12,21,22] For that purpose, active-ester-containing amphiphilic poly(methacrylate) block copolymers were self-assembled into polymer micelles, covalently conjugated with IMDQ, and then cross-linked to yield drug-loaded polymeric nanogels.[12,14]

Moreover, to prevent unfavorable nanotoxicities based on carrier accumulation in the body, nanogels were reversibly cross-linked with a pH-degradable ketal cross-linker that upon exposure to endosomal acidic environments afforded unimeric single-chain polymers that could be secreted renally.[23,24]

Received: February 11, 2020
Revised: April 6, 2020
Published: April 7, 2020

https://dx.doi.org/10.1021/acs.biomac.0c00205
Biomacromolecules 2020, 21, 2246−2257

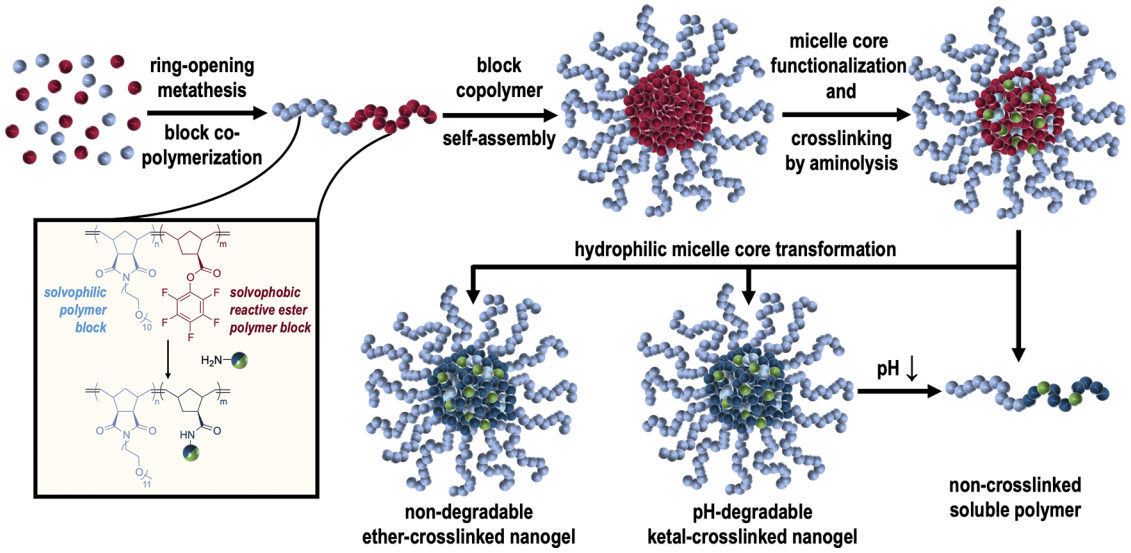

Figure 1. Synthetic concept for the fabrication of poly(norbornene)-based nanogels. *exo-N*-(Methoxypoly(ethylene glycol)) norbornene-dicarboxyimide and *exo*-norbornene-carboxylic acid-pentafluorophenyl ester are block copolymerized under ring-opening metathesis conditions. The resulting amphiphilic reactive ester block copolymers self-assemble in DMSO into precursor micelles, whose cores can be functionalized by mono-amine-bearing entities, cross-linked with pH-(non)-degradable bisamines, and finally converted into fully hydrophilic nanogels. Ketal cross-linking promotes pH-responsive particle disassembly upon exposure to endolysosomal pH affording single, non-cross-linked soluble polymers.

Interestingly, for the degraded nanogels or polymer chains, lymph node accumulation was significantly reduced; however, in in vitro cell studies, the immune stimulatory activity remained as high as for the intact nanogels.[21] In principle, a possible systemic inflammatory risk for the degraded polymer chains bearing IMDQ groups could therefore not be excluded. Thus, alternative strategies to omit the immune stimulation of the degraded particle or soluble single-chain polymers would be favorable to avoid unwanted side effects and result in not only spatial but also temporal control over the IMDQ activity.

For that purpose, we were interested in altering the design of IMDQ nanogel carrier systems that potentially meet these criteria. For a convenient block copolymer fabrication of well-defined polymers, the ring-opening metathesis polymerization (ROMP) reaction was chosen. In comparison to controlled radical polymerizations, ROMP enables a fast and effective one-pot block copolymerization within short reaction times.[25−27] Especially, the use of the fast initiating ruthenium metathesis catalyst (Grubbs third-generation catalyst) facilitates the production of low-polydispersity homo and amphiphilic block copolymers.[25]

In analogy to the previously investigated poly(methacrylamide) nanogels,[22,28,29] synthetic access to poly(norbornene)-based nanogels can be provided by copolymerizing mPEG and pentafluorophenyl esters containing norbornenes. The mPEG side chains in the solvophilic block should provide sufficient hydrophilicity and stealthlike shielding effect. The solvophobic block composed of pentafluorophenyl esters triggers phase separation and self-assembly into micelles in polar aprotic solvents like dimethyl sulfoxide (DMSO).[28] The reactivity of pentafluorophenyl esters to primary amines[30] guarantees a sequential covalent core modification with amine-modified IMDQs,[31] cross-linking with ketal bisamines, as well as conversion with hydrophilic amines, altogether affording pH-degradable nanogels, equipped with TLR7/8 agonists (Figure 1).

Interestingly, in this study, we observed that in contrast to ether- or ketal-cross-linked poly(norbornene)-based nanogels, the non-cross-linked hydrophilic block polymers covalently equipped with IMDQ did not stimulate the TLR-7/8. As they are also obtained upon intracellular degradation of the ketal-cross-linked nanogels, TLR7/8 immune stimulation is switched off upon particle degradation, thus making these systems highly attractive for spatial and temporal control over a precise IMDQ immune stimulation.

MATERIALS AND METHODS

Instrumentation. All ^{1}H nuclear magnetic resonance (NMR) spectra were recorded at room temperature on a Bruker 300 MHz or a 600 MHz FT NMR spectrometer (Bruker Avance III HD 300, Bruker Avance II 400, Bruker Avance III 600). Chemical shifts are provided in parts per million related to TMS. NMR spectra were processed with MestReNova 11.0.4 by Mestrelab Research. Samples were prepared in respective deuterated solvents, and their signals were referenced to the residual nondeuterated solvent signal. Diffusion ordered spectroscopy DOSY spectra were recorded at room temperature on a Bruker 400 MHz FT NMR spectrometer (Bruker Avance III HD 400) and processed by Bayesian DOSY transformation (minimum, 1.00×10^{-8}; maximum, 1.00×10^{-8}; resolution factor, 1.00; repetition factor, 1; points in dimension, 64).

Dynamic light scattering (DLS) experiments were performed on a Zetasizer Nano ZS (Malvern Instruments Ltd., Malvern, U.K.) equipped with a HeNe laser (λ = 633 nm) and detected at a scattering angle of 173° at 25 °C. The obtained data were processed by cumulant fitting for *z*-average and polydispersity index (PDI) as well as by CONTIN fitting for particle size distributions. Unless otherwise stated, dust was removed from the sample prior to each measurement by filtration through a GHP syringe filter (0.45 μm pore size, Acrodisc). Kinetic measurements of nanogel stability (in phosphate-buffered saline (PBS) pH 7.4) or degradation (in 100 mM acetate buffer, pH 5.0, prepared from a 1:1 mixture of 100 mM sodium acetate and 100 mM acetic acid) were recorded at time intervals of 5 min.

Size exclusion chromatography (SEC) characterization was conducted in hexafluoroisopropanol (HFIP) (containing 3.0 g/L of potassium trifluoroacetate) as eluent. The instrument was equipped with a PU 2080+ pump, an autosampler AS1555, and an RI detector RI2080+ from JASCO. Columns packed with modified silica were obtained from MZ-Analysentechnik: PFG columns; particle size, 7

https://dx.doi.org/10.1021/acs.biomac.0c00205
Biomacromolecules 2020, 21, 2246−2257

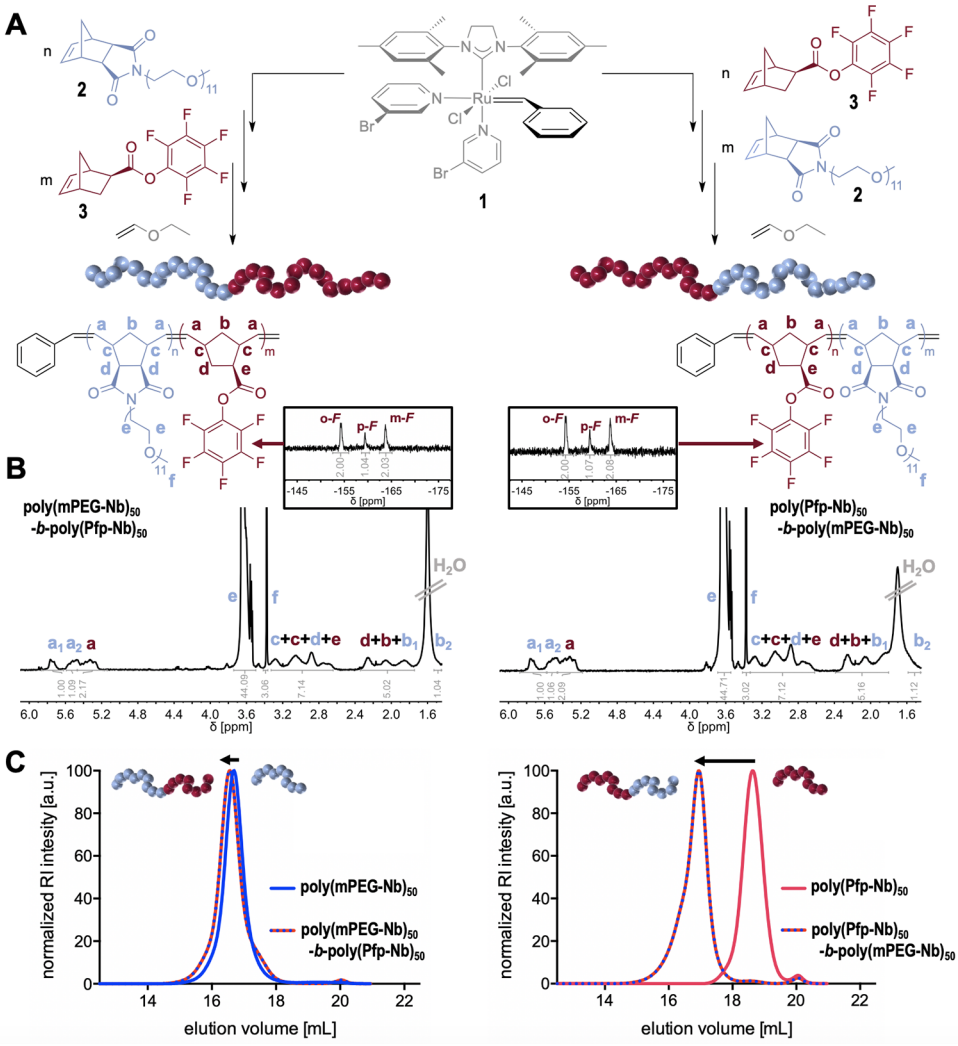

Figure 2. (A) Synthetic scheme for different polymerization sequences of **poly(mPEG-Nb)-*b*-poly(Pfp-Nb)** block copolymers. *exo*-*N*-(Methoxypoly(ethylene glycol)) norbornene-dicarboxyimide **2** and *exo*-norbornene-carboxylic acid-pentafluorophenyl ester **3** are block copolymerized under ring-opening metathesis conditions catalyzed by the fast initiating ruthenium metathesis catalyst **1** (Grubbs third-generation catalyst). (B) ^{1}H NMR and ^{19}F NMR (black box) of the isolated **poly(mPEG-Nb)-*b*-poly(Pfp-Nb)** block copolymers. (C) SEC traces of the respective block- and homopolymers with hexafluoroisopropanol (HFIP) as eluent.

μm; porosity, 100 and 1000 Å. Calibration was carried out with poly(methyl methacrylate) (PMMA) standards, purchased from PSS, Mainz.

Matrix-assisted laser desorption ionization time-of-flight (MALDI-ToF) mass spectra were acquired on a rapifleXTM MALDI-ToF/ToF mass spectrometer from Bruker equipped with a 10 kHz scanning smartbeam three-dimensional (3D) laser (Nd:YAG at 355 nm) and a 10 bit 5 GHz digitizer. Measurements were performed in a positive reflector mode using DCTB (*trans*-2-[3-(4-^{t}butylphenyl)-2-methyl-2-propenylidene]malononitrile) acid as a matrix and the obtained data processed by mMass software.

Transmission electron microscopy (TEM) images were prepared by adding 4 μL of the nanogel/polymer solution at 2 mg/mL in water (supplemented with 0.1% conc. aqueous ammonia) onto a carbon-coated copper grid. After drying in air for 10 min, the remaining solution was removed by a filter paper. After further drying in air, the measurement was conducted on a JEOL JEM-1400 TEM operating at an accelerating voltage of 120 kV.

UV−vis spectra were recorded on a Jasco V-630 spectrophotometer equipped with a Peltier thermostatted single-cell holder (JASCO ETC-717) cooled by a water thermostat (A. Knüss Optronic V50) to guarantee measurement conditions at 25.0 °C.

Fluorescence and cell assay recorded absorbance intensities were also monitored on a Tecan Spark 20 M microplate reader.

Flow cytometry analyses were performed on a BD Accuri, and the obtained data were processed using the FlowJo software package.

Fluorescence nonconfocal microscopy images were recorded on a Leica DMi8 microscope with a 100× oil immersion objective. Fluorescence confocal laser scanning microscopy images were recorded on a Leica SP5 confocal microscope system with a 63× oil immersion objective. All images were processed by ImageJ software.

Materials. Unless otherwise mentioned, all chemicals were purchased from Sigma-Aldrich, Tokyo Chemical Industry, or Acros Organics and used as received. 1-(4-(Aminomethyl) benzyl)-2-butyl-1*H*-imidazo[4,5-*c*]quinolin-4- amine (IMDQ) could be provided according to an earlier report.[31] Dialysis was performed using Spectra/Por 3 membranes obtained from Spectrum Labs with a molecular weight cutoff of 1000 g/mol.

Dulbecco's phosphate-buffered saline (PBS), cell culture medium, and supplements were purchased from Thermo Fisher. The RAW-Blue reporter cell line and QUANTI-BlueTM were obtained from InvivoGen.

Monomer Synthesis. *Synthesis of exo-N-(Methoxypoly-(ethylene glycol)) Norbornene-dicarboxyimide **2**.* The synthesis of

https://dx.doi.org/10.1021/acs.biomac.0c00205
Biomacromolecules 2020, 21, 2246−2257

the solvophilic mPEG-containing monomer was adapted from the literature[32] (Scheme S1). A solution of *exo*-[2.2.1]bicyclo-2-ene-5,6-dicarboxylic anhydride (0.43 g, 2.61 mmol, 1.0 equiv) and mPEG-amine 0.5 kDa (1.34 g, 2.61 mmol, 1 equiv) in toluene (50 mL) was heated at reflux overnight. The reaction mixture was then cooled to room temperature, and the solvent was evaporated under reduced pressure. The crude reaction product was purified via column chromatography ($CHCl_3$/MeOH 10:1). Product **2** was obtained as a yellow oil in 95% yield (1.64 g, 2.51 mmol).

^{1}H NMR (300 MHz, $CDCl_3$) δ [ppm] = 6.26 (t, J = 1.9 Hz, 2H), 3.71−3.49 (m, 44H), 3.36 (s, 3H), 3.25 (p, J = 1.7 Hz, 2H), 2.66 (d, J = 1.3 Hz, 2H), 1.47 (dt, J = 9.8, 1.6 Hz, 1H), 1.34 (dt, J = 9.9, 1.6 Hz, 1H) (Figures S1 and S3).

^{13}C NMR (75 MHz, $CDCl_3$) δ [ppm] = 178.12, 137.93, 72.03, 70.68, 69.96, 66.99, 59.14, 47.92, 45.37, 42.82, 37.8 (Figures S2, S4, and S5).

Synthesis of exo-Norbornene-carboxylic Acid-Pentafluorophenyl Ester **3**. The procedure was adapted from the literature[33] (Scheme S2). Pentafluorophenol (2.62 g, 18.9 mmol, 1 equiv) and *exo*-[2.2.1]bicyclo-2-ene-5-carboxylic acid (3.84 g, 20.8 mmol, 1.1 equiv) (that was first isolated from a mixture of *exo* and *endo* species—compare Supporting Information and Scheme S2) were dissolved in anhydrous dichloromethane (DCM) (25 mL) and cooled to 0 °C. Dicyclohexylcarbodiimide (DCC) (4.31 g, 20.9 mmol, 1.1 equiv) was added to the solution, and dimethylaminopyridine (DMAP) (0.23 g, 1.9 mmol, 0.1 equiv) dissolved in anhydrous DCM (2 mL) was added slowly via a syringe. After 1 h, the reaction mixture was allowed to warm to room temperature and stirred overnight. After 20 h, the volatiles were removed in vacuo and the crude reaction mixture was purified by column chromatography (^{C}Hex/EtOAc 20:1) to yield 5.19 g (17.1 mmol, 90.3%) of **3** as a pale yellow oil.

^{1}H NMR (300 MHz, $CDCl_3$): δ 6.23 (dd, J = 5.7, 2.9 Hz, 1H,), 6.18 (dd, J = 5.7, 3.0 Hz, 1H), 3.27 (ddq, J = 3.1, 1.5, 0.8 Hz, 1H), 3.03 (s, 1H), 2.59 (ddd, J = 9.0, 4.5, 1.5 Hz, 1H), 2.16−1.89 (m, 1H), 1.60−1.55 (m, 1H), 1.54 (t, J = 1.7 Hz, 1H), 1.52−1.47 (m, 1H) (Figures S6 and S8).

^{13}C NMR (75 MHz, $CDCl_3$): δ 172.56, 138.68, 135.46, 47.16, 46.54, 42.87, 41.95, 30.88 (Figures S7, S9, and S10).

^{19}F NMR (376 MHz, $CDCl_3$) δ −154.26 (d, J = 17.7 Hz), −159.52 (t, J = 21.7 Hz), −163.64 (dd, J = 22.0, 17.6 Hz) (Figure S11).

Polymerization Procedure. The procedure was adapted from the literature and modified.[26] In an exemplified procedure, the block copolymer synthesis of **poly(mPEG-Nb)$_{50}$-*b*-poly(Pfp-Nb)$_{50}$** is described: 0.13 mL of a 0.14 M stock solution of *exo-N*-(methoxypoly(ethylene glycol)) norbornene-dicarboxyimide **2** (0.068 mmol, 44.0 mg, 65 equiv) in DCM was rapidly transferred to a flame-dried Schlenk tube charged with 0.11 mL of a 0.13 M stock solution of ruthenium initiator Grubbs third-generation catalyst **1** (0.001 mmol, 1.2 mg, 1.3 equiv) in DCM. After thin-layer chromatography (TLC) showed a full conversion of *exo-N*-(methoxypoly(ethylene glycol)) norbornene-dicarboxyimide **2**, an aliquot of the reaction mixture was removed (0.13 mL, corresponding to 0.3 equiv of ruthenium initiator), terminated with ethyl vinyl ether (EVE), and characterized by NMR spectroscopy and size exclusion chromatography (SEC) (Figures S12 and S13). Then, 0.38 mL of a 0.14 M stock solution of *exo*-norbornene-carboxylic acid-pentafluorophenyl ester **3** (0.053 mmol, 16.0 mg, 50 equiv) in DCM was added to the reaction vial to proceed block copolymerization. After full second monomer consumption, as indicated by TLC, the reaction was terminated by the addition of an excess of EVE. The resulting block copolymer **poly(mPEG-Nb)$_{50}$-*b*-poly(Pfp-Nb)$_{50}$** was precipitated three times into cold hexane. Hexane was decanted, and the obtained material was dried in vacuo. The polymers were analyzed by SEC, ^{1}H NMR, and ^{19}F NMR (Figures 2, S14, and S15).

^{1}H NMR (300 MHz, $CDCl_3$): δ 5.85−5.65 (br, 1H,), 5.60−5.45 (br, 1H), 5.45−5.20 (br, 2H), 3.71−3.49 (m, 44H), 3.36 (s, 3H), 3.33−2.60 (m, 7H), 2.35−1.75 (m, 5H), 1.55−1.47 (br, 1H) (Figure 2B).

^{19}F NMR (375 MHz, $CDCl_3$): δ −154.35 (br, 2H), −159.48 (br, 1H), −163.84 (br, 2H) (Figure S2B).

Nanogel Formation. *Block Copolymer Self-Assembly.* The desired block copolymer (10 mg, 13.6 μmol reactive ester for **poly(mPEG-Nb)$_{50}$-*b*-poly(Pfp-Nb)$_{50}$**) was dispersed in anhydrous DMSO, yielding a 10 mg/mL solution. Subsequent sonication (1−8 h) resulted in the formation of self-assembled polymeric micelles, as verified by DLS measurements, and micellar dispersions were used for further nanogel synthesis.

Core Functionalization of Polymeric Micelles. The synthesis of three different types of nanogels (ketal-cross-linked, ether-cross-linked, and non-cross-linked) was performed by dispersing the desired amount of pentafluorophenyl ester-containing polymeric micelle (1 mL, 13.6 μmol reactive ester) in anhydrous DMSO in a flame-dried Schlenk tube. The desired cross-linkers were added together with triethylamine (0.61 mL of a 1.38 mg/mL stock solution, 8.3 μmol, 0.61 equiv) under a nitrogen atmosphere. The equivalents are depicted in reference to amine functionality. 2,2-Bis(aminoethoxy)-propane (0.6 mL of a 1.10 mg/mL stock solution, 4.1 μmol, 0.6 amine equiv) was used for ketal cross-linking, while 1,2-bis(aminoethoxy)-ethane (0.6 mL of a 1.01 mg/mL stock solution, 4.1 μmol, 0.6 amine equiv) served as an ether cross-linker. In the case of non-cross-linking, monomethoxy-poly(ethylene glycol)-amine 0.75 kDa (0.6 mL of a 10.21 mg/mL stock solution, 8.2 μmol, 0.6 amine equiv) was added. The reaction mixture was stirred for 1 day at 40 °C. For the complete removal of residual pentafluorophenyl reactive esters, the reaction was quenched by the addition of monomethoxy-poly(ethylene glycol)-amine 0.75 kDa (1.0 mL of a 10.21 mg/mL stock solution, 13.6 μmol, 1.0 amine equiv) and triethylamine (1.1 mL of a 1.38 mg/mL stock solution, 15.0 μmol, 1.1 equiv) and stirred at room temperature for 1 day. Nanogels were then transferred into dialysis membranes (MWCO: 3.5 kDa) and dialyzed against 1 L of water with 0.1% ammonia for 3 days, changing the water two times per day. Lyophilization afforded nanogels as colorless to brownish gooey materials. The cross-linked particles were significantly more solid than the non-cross-linked polymers, which were obtained as highly viscous oils.

Fluorescently Labeled Nanogels. To 1 mL of the precursor polymer (10 mg, 13.6 μmol reactive ester for **poly(mPEG-Nb)$_{50}$-*b*-poly(Pfp-Nb)$_{50}$**) in anhydrous DMSO was added Oregon Green cadaverine (14 μL of a 2.5 mg/mL stock solution in DMSO, 68 nmol; 0.005 equiv) and dry triethylamine (TEA) (10 μL of a 1.38 mg/mL stock solution in DMSO, 136 nmol, 0.01 equiv) and stirred overnight under a nitrogen atmosphere. After dye conjugation, the polymer cross-linking was performed in analogy to the procedure described above. Note that beyond dialysis, an additional spin filtration was conducted to remove all residual free dye (MWCO 10 kDa, 0.1% NH_3-aqueous solution/MeOH 1:1), as confirmed by the quantitative reversed-phase thin-layer chromatography (RP-TLC) (Figures S26−S28).

IMDQ Conjugation to Nanogels. To 1 mL of the precursor polymer (10 mg, 13.6 μmol reactive ester for **poly(mPEG-Nb)$_{50}$-*b*-poly(Pfp-Nb)$_{50}$**) in anhydrous DMSO were added IMDQ (0.1 mL of a 10 mg/mL stock solution in DMSO, 2.3 μmol; 0.17 equiv) and dry TEA (0.2 mL of a 1.38 mg/mL stock solution in DMSO, 2.7 μmol, 0.2 equiv) and stirred overnight under a nitrogen atmosphere. After drug conjugation, the polymer cross-linking was performed in analogy to the procedure described above. Here, beyond dialysis, additional spin filtration was not necessary to remove all residual free drug, as confirmed by quantitative reverse phase thin-layer chromatography (RP-TLC) (Figures S34−S36).

Cellular Uptake, TLR Stimulation, and Viability. RAW-Blue macrophages were cultured in Dulbecco's modified Eagle's medium (DMEM) supplemented with 10% fetal bovine serum, 2 mM L-glutamine, 1 mM sodium pyruvate, 1% penicillin/streptomycin, 0.01% normocin, and 0.02% zeocin as selection medium. The cells were kept at 37 °C with 5% CO_2 saturation.

RAW-Blue Macrophage TLR Reporter Assay. IMDQ TLR receptor stimulation followed by NF-kB/AP-1 activation was monitored by secretion of embryonic alkaline phosphatase from RAW-Blue cells, as recommended by the manufacturer (InvivoGen). The RAW-Blue cells were seeded into 96-well plates at a density of 90 000 cells/well in 180

https://dx.doi.org/10.1021/acs.biomac.0c00205
Biomacromolecules 2020, 21, 2246−2257

μL of culture medium. Each well was treated with 20 μL of a nanogel sample at the given final IMDQ concentrations (and corresponding empty nanogel or other control concentrations). After incubation for 18 h, 50 μL of the supernatant from each well was collected and tested for secreted embryonic alkaline phosphatase (SEAP) using the QUANTI-Blue assay (InvivoGen). QUANTI-Blue (150 μL) was added to each sample and incubated at 37 °C. SEAP levels were determined by measuring the optical density at 615 nm using a microplate reader. The activity was determined by an increase in the optical density relative to the negative control treated with PBS. All experiments were conducted at $n = 4$.

3-(4,5-Dimethylthiazol-2-yl)-2,5-diphenyltetrazolium Bromide (MTT) Assay. 3-(4,5-Dimethylthiazol-2-yl)-2,5-diphenyltetrazolium bromide (MTT) (50 μL, 0.5 mg/mL in PBS) was added to the RAW-Blue cells that were treated with nanogel samples at the given final IMDQ concentrations (and corresponding empty nanogel concentrations), as described before. After an incubation period of 2−3 h, the formed formazan crystals were dissolved by the addition of 100 μL 10% m/v SDS/0.01 M HCl and incubated overnight at 37 °C. Quantification was done by measuring the absorbance at 570 nm using a microplate reader.

Flow Cytometry. RAW-Blue macrophages were seeded into 24-well titer plates (250 000 cells/well, suspended in 0.90 mL of culture medium) and incubated overnight to allow cell sedimentation and subsequent adhesion to the bottom of the wells. Next, the cells were incubated with 100 μL of Oregon Green labeled nanogel or polymer solution in PBS (yielding a total polymer/nanogel concentration of either 30 or 100 μg/mL). All samples were run in triplicate, and the experiment was conducted for 18 h at 37 °C. The cell culture medium was then aspirated, and the cells were washed with 1 mL of PBS and incubated with 400 μL of a cell dissociation buffer (15 min, 37 °C). The cell suspensions were then diluted with 400 μL of cell culture medium, transferred into Eppendorf tubes, and centrifuged immediately (350*g*, 10 min, 5 °C). Finally, the supernatant was aspirated and the cell pellets were suspended in 250 μL of PBS. They were kept on ice to maintain cell integrity prior to flow cytometric analysis performed on a BD Accuri C6 (BD Biosciences). The data were processed by FlowJo software.

Fluorescence Microscopy. RAW-Blue macrophages were seeded in an Ibidi μ-slide eight-well confocal microscopy chamber (50 000 cells/well, suspended in 0.18 mL of the culture medium) and left to adhere overnight. Next, the cells were incubated with 20 μL of Oregon Green labeled nanogel or polymer solution in PBS (yielding a total polymer/nanogel concentration of 100 μg/mL) for 24 h. Then, the culture medium was aspirated and the cells were washed three times with PBS. Next, 200 μL of 4% paraformaldehyde was added and allowed to fixate for 15 min at 37 °C. Afterward, the cells were washed again three times with PBS and their nuclei were stained with 200 μL of 4′,6-diamidino-2-phenylindole (DAPI) (80 μg/mL in PBS) for 10 min at 37 °C. Finally, the cells were washed once more three times with PBS and then stored under an aqueous mounting medium. First, nonconfocal fluorescence microscopy images were recorded on a Leica DMi8 microscope with a 100× oil immersion to confirm particle or polymer uptake. Then, to prove internalization of the material into the cells, fluorescence confocal laser scanning microscopy images were recorded on a Leica SP5 confocal microscope system with a 63× oil immersion objective. All images were finally processed by the ImageJ software package.

RESULTS AND DISCUSSION

We previously reported on immune stimulatory nanogels, based on reactive amphiphilic poly(methacrylamide) block copolymers derived from mPEG- and pentafluorophenyl ester-bearing acrylates, that can be prepared by RAFT polymerization and subsequent versatile postpolymerization modification.[22] Prior to this study, we investigated other polymerization techniques and monomer systems and thereby observed that, in analogy to our previously reported studies, the ring-opening metathesis polymerization (ROMP) of norbornenes with mPEG or pentafluorophenyl ester side chains can provide rapid access to highly modifiable, pH-degradable nanogels. In this study, we introduce this carrier system for the first time and observed that covalent modification with the TLR7/8 agonist IMDQ[31] provides immune stimulatory properties only for the intact particles, while converted into single polymer chains, a loss in activity and conversion into immunologically silent species make the whole delivery system highly attractive for clinical purposes.

Synthesis of Poly(norbornene) Precursor Block Copolymers. Due to their high activity during metathesis reactions, substituted *exo*-norbornenes were chosen as monomers and derivatized to provide characteristics for amphiphilic reactive ester block copolymers. The attachment of an mPEG-amine to norbornene dicarboxylic anhydride provides access to the solvophilic monomer **2**. Furthermore, PEG is known for its biocompatibility and stealth effect in vivo, which is a vital feature in achieving long blood circulation times.[34−36] Alternatively, norbornene carboxylic acid-pentafluorophenyl ester **3** serves as an amine reactive precursor, and due to its highly fluorinated character, it additionally provides phase separation properties in polar aprotic media.[11]

A scheme for the syntheses of the monomers can be found in the Supporting Information (Schemes S1 and S2). *N*-(Poly(ethylene glycol))-*cis*-5-norbornene-*exo*-2,3-dicarboximide **2** was directly accessed starting from commercially available *exo*-norbornene carboxylic anhydride. Upon condensation reaction with an amino-capped methoxy-poly(ethylene glycol) in toluene, *exo*-imide **2** was obtained in nearly quantitative yield and confirmed by ^{1}H and ^{13}C NMR, as well as COSY, HSQC, and HMBC measurements (Figures S1−S5).

In general, exo-isomers are usually the ones with higher reactivity during ROMP;[37−40] however, toward the synthesis of *exo*-norbornene-5-carboxylic acid-pentafluorophenyl ester **3**, the starting material norbornene-5-carboxylic acid is only commercially available as a mixture of 80% endo-isomer and 20% exo-isomer, as determined by ^{1}H NMR. However, when treated with iodine and KI, the formation of an iodolactone is possible, yet, exclusively for the endo-acid. Consequently, in a simple purification step, the exo-acid could be extracted from the endo-derived iodolactone, as described in the Supporting Information, and subsequently esterificated with pentafluorophenol under Steglich conditions with DCC and DMAP.[41,42] The resulting *exo*-norbornene-5-carboxylic acid-pentafluorophenyl ester **3** was obtained in 90% yield and characterized by ^{1}H, ^{13}C, and ^{19}F NMR, as well as COSY, HSQC, and HMBC measurements (Figures S6−S11).

For the controlled synthesis of homo and block copolymers, the fast initiating bromopyridine ruthenium catalyst **1** was chosen (Figure 2A). The high functional group tolerance and especially the fast initiation kinetics of the ruthenium complex during ROMP[43] enables living polymerization conditions and narrow molecular weight distributions.[25] Due to the living nature, block copolymers could, therefore, be obtained directly in a one-pot manner after full first block monomer consumption. Here, the monomer conversion was monitored by TLC and NMR analyses to be nearly quantitative, which shows the high activity of the catalyst and the norbornene monomers.

Consequently, molecular weights could be easily tuned by adjusting the initiator-to-monomer ratio (e.g., compare SEC traces of the homopolymers of **2** in Figure S13), and the

https://dx.doi.org/10.1021/acs.biomac.0c00205
Biomacromolecules 2020, 21, 2246−2257

resulting polymers provide a high end-group fidelity, as confirmed by their MALDI spectra (Figure S12A−C).

As homopolymers from monomer **2** were prepared readily, block copolymerization was subsequently performed by adding Pfp monomer **3** to the reaction vessel after a complete monomer conversion. Also, the reverse polymerization sequence was conducted successfully and afforded block copolymers of similar properties (Figure 2A). Different molecular weights of homo and block copolymers could be obtained and successfully characterized by ^{1}H NMR, ^{19}F NMR, and SEC analyses (Figures 2B,C and S14). Broad signals at δ = 5.8−5.2 indicate the appearance of polymeric olefinic protons. The signal at δ = 5.8 was assigned to the solvophilic block and used to calculate the block ratio. The signal of the olefinic protons at δ = 3.4 verifies the incorporation of the mPEG side chain, and the appearance of broad signals in the ^{19}F NMR spectra shows the polymerization of the solvophobic Pfp monomer **3** (Figure 2B). The shift in the elution volume for the subsequent polymerization of solvophilic monomer **2** onto a block of monomer **3** is significantly larger than for the reverse polymerization sequence due to the difference in molecular weight of the incorporated monomers themselves (Figure 2C). Further confirmation of complete chain extension could be derived from diffusion ordered NMR spectroscopy (DOSY) measurements (Figure S15). A complete shift of diffusion units for all proton signals in the NMR spectra from the homo to block copolymer confirmed the successful block copolymer formation.

The molecular weight of the block copolymer could be varied from 22 to 190 kDa by adjusting the monomer-to-initiator ratio. Also, polymers with different block ratios (as determined by ^{1}H NMR) could be prepared successfully. The results are all summarized by Table 1.

Table 1. SEC Characterization of Block Copolymers

polymer	M_n (theo.)	M_n (SEC)[a]	PDI (SEC)[a]
poly(mPEG-Nb)$_{10}$-*b*-poly(Pfp-Nb)$_{50}$	21 775	56 000	1.15
poly(mPEG-Nb)$_{20}$-*b*-poly(Pfp-Nb)$_{50}$	28 235	70 000	1.21
poly(mPEG-Nb)$_{50}$-*b*-poly(Pfp-Nb)$_{50}$	47 615	117 000	1.28
poly(Pfp-Nb)$_{50}$-*b*-poly(mPEG-Nb)$_{50}$	47 615	99 000	1.27
poly(mPEG-Nb)$_{100}$-*b*-poly(Pfp-Nb)$_{100}$	95 125	145 000	1.34
poly(mPEG-Nb)$_{200}$-*b*-poly(Pfp-Nb)$_{200}$	190 146	198 000	1.59

[a]Determined by HFIP-SEC (PMMA standard).

Interestingly, all block copolymers could be readily prepared with reaction times ranging from 10 to 30 min per block. This is one of the most significant advantages compared to the more difficult and longer (usually days) reaction procedures necessary for controlled radical block copolymerization processes. Moreover, the block copolymerization could be conducted in a one-pot manner and, thus, only a single purification step was required to isolate the precursor block copolymers for the subsequent nanogel fabrication.

Self-Assembly of Poly(norbornene) Precursor Block Copolymers. In analogy to the previously published poly(methacrylamide) nanogels, the poly(norbornene)-based block copolymers were tested for their phase separation and self-assembling behavior in polar aprotic solvents. The solvophobic pentafluorophenyl ester moiety is again immiscible with most polar aprotic solvents including DMSO and, thus, enables microphase separation and self-assembly of the block copolymers into active-ester-containing polymeric micelles.

With increasing molecular weights of the respective block copolymers, the size of the obtained precursor micelles increases. The adjustment of particle size is, therefore, conveniently achieved by variation of the monomer-to-initiator ratio during the synthesis of the block copolymers. The differently composed micelles in DMSO were characterized by dynamic light scattering (DLS), and the results are shown in Figure 3.

The self-assembly of the obtained polymers provided differently sized micelles in the range of 40−190 nm depending on the molecular weight and block ratios of the respective polymer. With increasing molecular weight but the same 1:1 block ratio, the size of the polymeric micelles increases (as shown in Figure 3A). By reducing the molecular weight of the solvophilic mPEG-containing block, the size of the obtained particles decreases and the PEG corona becomes smaller (as shown in Figure 3B).

Synthesis Poly(norbornene)-Based Nanogels. The active-ester-containing polymeric micelles were then treated with various bisamines as cross-linking agents to stabilize their morphology while changing the core polarity from hydrophobic to hydrophilic. A ketal-bond-containing bisamine should introduce a pH-sensitive trigger for the disassembly of the nanogels, whereas an ether-bond-containing bisamine should be insensitive toward acidic media. Furthermore, residual Pfp ester moieties, after cross-linking, were first substituted with ethanolamine. The small hydroxy group-bearing amine was chosen as a solubilizing group in analogy to the known poly(methacrylamide) systems. However, due to the high hydrophobicity of the hydrocarbon backbone, the non-cross-linked polymers still showed micellar self-assembly in PBS after ethanolamine treatment (Figure S16). Only when dispersed in DMSO, single polymer chains could be monitored (Figure S17). For the nanogels, ketal cross-linking could be degraded under acidic conditions in DMSO (Figure S18).

Therefore, in subsequent experiments, treatment with ethanolamine was replaced by a short oligomer mPEG-amine (0.75 kDa) to assure increasing nanogel core polarity and single-chain solubility for the non-cross-linked version. Altogether, Pfp ester substitution of cross-linked and non-cross-linked particles with the hydrophilic mPEG-amine (Figure 4A) lead to fully water-soluble polymers and degradation of ketal-cross-linked particles under mild endosomal acidic media, as monitored by DLS measurements (Figure 4B).

Moreover, covalent core cross-linking of the self-assembled block copolymer micelles was further confirmed by transmission electron microscopy (TEM) of samples drop-cast onto the grids (Figure 4C and Supporting Information Figures S19−S21). Only for the core-cross-linked nanogels, particular structures with a high electron density could be visualized. For the **poly(Pfp-Nb)$_{50}$-*b*-poly(mPEG-Nb)$_{50}$**-derived ether-cross-linked nanogels, sizes of around 20−60 nm were found, while the non-cross-linked species provided only structures below 15 nm representing single polymer chains (Figure 4C2). Interestingly, for the ether-cross-linked nanogels, also a core−shell-like morphology was fairly visible (Figure 4C1).

To further study the nanoparticle behavior upon exposure to extracellular and endolysosomal pH over time, samples were

https://dx.doi.org/10.1021/acs.biomac.0c00205
Biomacromolecules 2020, 21, 2246−2257

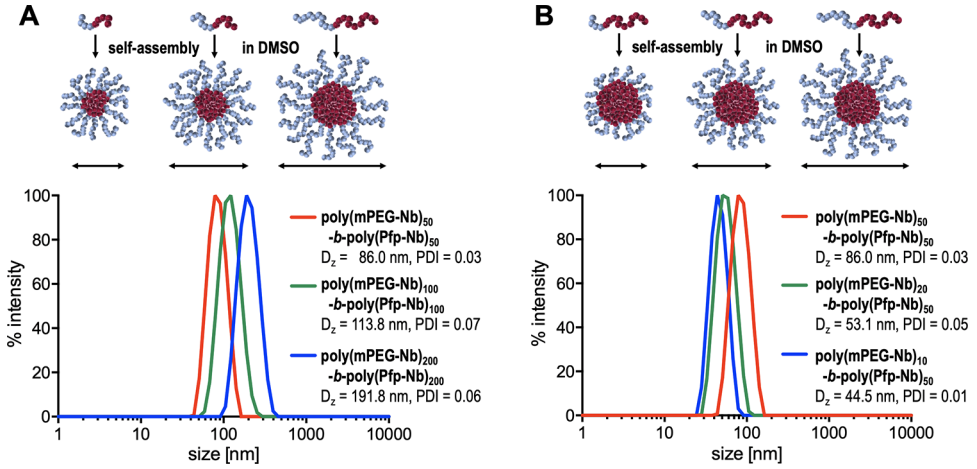

Figure 3. DLS measurements of self-assembling **poly(mPEG-Nb)-*b*-poly(Pfp-Nb)** block copolymers in DMSO. (A) Polymeric micelles, obtained from block copolymers with increasing molecular weight and 1:1 block ratios. (B) Polymeric micelles obtained from block copolymers with decreasing molecular weight of the solvophilic block but the same solvophobic block.

prepared at 1 mg/mL in PBS at pH 7.4 or in 100 mM acetate buffer at pH 5.0 and continuously monitored by DLS measurements. Only for the ketal-cross-linked nanogels at pH 5.0, a decrease in count rate and a shift in particle size and distribution toward smaller non-cross-linked soluble polymers were found, while the particles remained stable in PBS for 24 h (Figure 4D). Ether-cross-linked nanogels retained their scattering intensity and size distribution in both media as well as the non-cross-linked soluble polymers (Figures S22–S24). In analogy to our previous studies,[23] these results confirm that nanogel unfolding for ketal-cross-linked polymer micelles into single polymer chains can only occur intracellularly at endolysosomal pH, but they remain intact at neutral physiological pH.

Immune Stimulatory Properties of IMDQ-Loaded Poly(norbornene)-Based Nanogels. Due to the pentafluorophenyl ester approach, pharmacologically active molecules or fluorogenic tracer molecules with a single primary amine can easily be attached via amide formation into the micelle core for both therapeutic and diagnostic purposes. Especially for immunodrug delivery, nanocarriers with sizes smaller than 100 nm and sufficient PEG shielding provide ideal properties to, e.g., efficiently reach and accumulate in draining lymph nodes.[21] For that purpose, the **poly(mPEG-Nb)$_{50}$-*b*-poly(Pfp-Nb)$_{50}$** block copolymer system was chosen and converted into degradable or nondegradable nanogels and soluble polymers (Figures 3A and 4B) for the following immunodrug delivery studies (Figures 5 and 6).

To first investigate cellular toxicity and uptake, precursor micelles were treated with the amine-bearing fluorescent dye Oregon Green cadaverine (Figure 5A) prior to cross-linking with ketal- or ether-containing bisamines, as well as hydrophilization with mPEG-amine (Figure S25). Purification was conducted by dialysis and spin filtration to remove all residual free dye (MWCO 10 kDa, 0.1% NH_3 aqueous solution/MeOH 1:1) and confirmed by quantitative reversed-phase thin-layer chromatography (RP-TLC) (Figures S26–S28). The resulting core-cross-linked nanogels or soluble polymer were all equipped with Oregon Green as fluorescent tracer (Figure 5A–C).

The particles and polymers did not significantly differ in size from species prepared without dye (Figure 5B), as determined by DLS characterization in PBS, yet successful conjugation was verified by UV–vis spectroscopy showing similar absorbance maxima around 500 nm (Figure 5C).

All particles and polymers did not exhibit any major influence on cell viability, as verified by MTT assay with RAW-Blue macrophages at a particle concentration of up to 100 mg/L (Figure 5D). The RAW-Blue cell line was used in this study as a model cell line for antigen-presenting cells, which even allow a rapid screening of immune cell maturation by the secretion of an embryonic alkaline phosphatase. This was chromosomally integrated into this model cell line, and upon TLR7/8 stimulation followed by NF-kB and AP-1 signaling, it is secreted into the cell supernatant and can be quantified spectrophotometrically as an indicator for immune stimulation.

This cell line was further used to study the uptake of the Oregon Green labeled species using flow cytometry and fluorescence (confocal) microscopy. RAW-Blue macrophages were treated with similar amounts of material, as referred to the absorbance/fluorescence intensities of Oregon Green (Figure S29). Ketal- or ether-cross-linked nanogels (30 and 100 μg/mL, respectively) as well as non-cross-linked soluble polymers were applied to the cells and incubated for 24 h prior to flow cytometric analysis (its gating strategy can be found in Figure S30). The resulting histograms in Figure 5E1 and mean fluorescence intensities in Figure 5E2 show moderate but similar cell uptake for all different nanogel and polymer species. This uptake was also dose-dependent and could be increased for the incubation concentration from 30 to 100 μg/mL.

These findings could also be confirmed by fluorescence microscopy, where an association of Oregon Green labeled material was observed for the RAW-Blue macrophages treated with all three different species for 24 h at 100 μg/mL (Figure S31). Through confocal laser scanning microscopy, an intracellular localization of the nanogels or soluble polymers by the presence of Oregon Green labeled species insides cells was found (Figures 5F and S32), indicating identical internalization of all species into the cells probably via endocytotic pathways.

In analogy to the preparation of these nontoxic dye-functionalized nanogels and soluble polymers, similar fabrication conditions were applied for the conjugation of the small-molecule imidazoquinoline TLR agonist IMDQ[31] to

https://dx.doi.org/10.1021/acs.biomac.0c00205
Biomacromolecules 2020, 21, 2246–2257

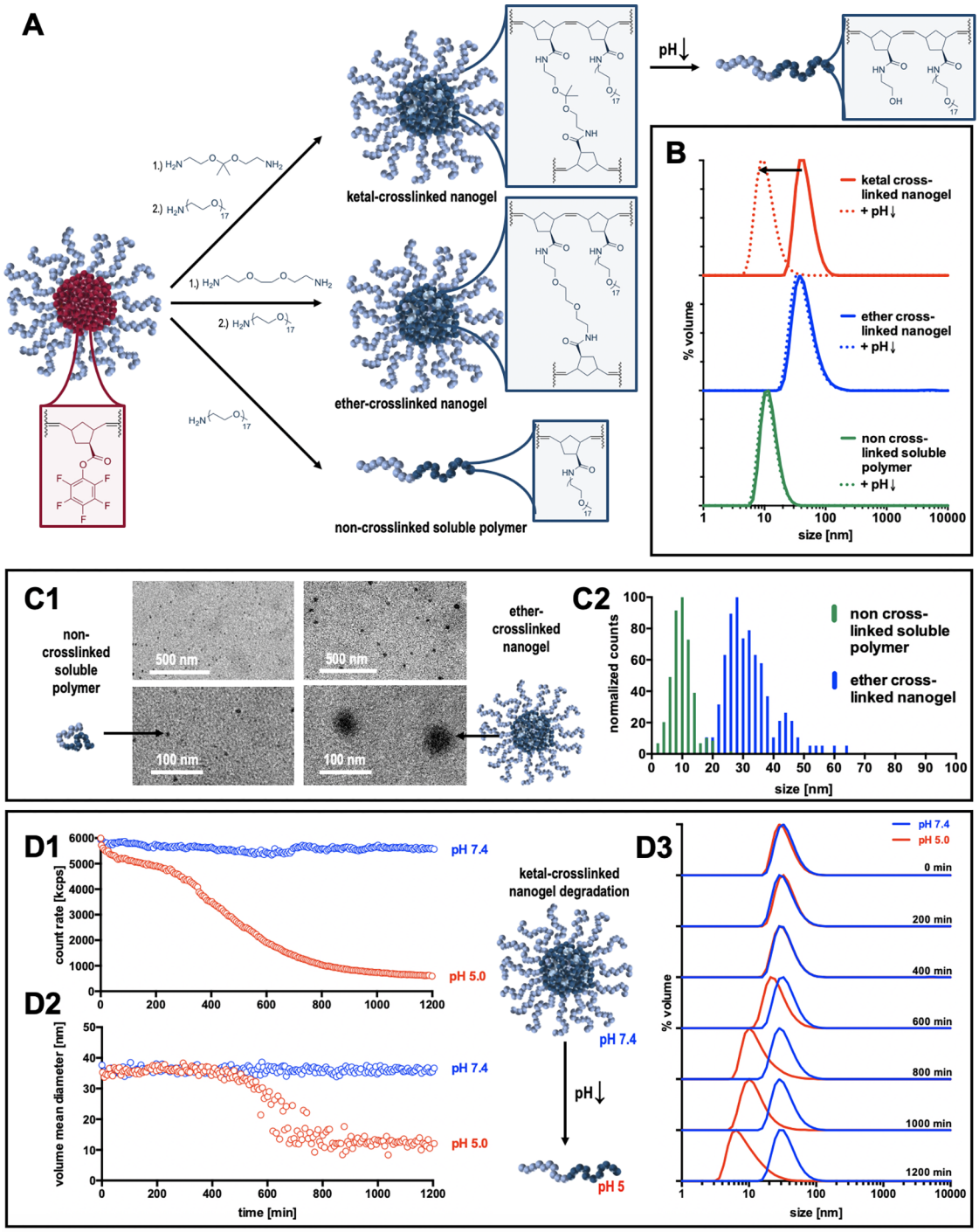

Figure 4. (A) Substitution of Pfp esters with bisamine cross-linkers and/or short oligo mPEG amines affording hydrophilic nanogels/water-soluble polymer chains. (B) DLS characterization of the resulting cross-linked nanogels and non-cross-linked polymers in PBS derived from **poly(Pfp-Nb)$_{50}$-*b*-poly(mPEG-Nb)$_{50}$** precursor micelles, as well as their response upon lowering the pH to endosomal levels of pH 5. Note that only the ketal-cross-linked nanogels disassemble into single polymer chains exclusively. (C) TEM images of soluble polymer chains and nondegradable ether-cross-linked nanogels (1) and their derived counted size distributions (2). (D) DLS monitoring of ketal-cross-linked particle stability at extracellular pH and degradation at endolysosomal pH. Particle scattering intensity (1), particle size (2), and size distribution (3) decrease over time under mild acidic conditions (100 mM acetate buffer, pH 5.0), while the ketal-cross-linked particle's integrity is guaranteed under neutral conditions (PBS, pH 7.4) for 24 h (compare also Figures S22–S24).

improve its pharmacokinetic behavior. Prior to cross-linking and hydrophilization with mPEG-amine, the substitution of Pfp units with the amine-containing IMDQ was performed (Figure S33). After purification by excessive dialysis, IMDQ-conjugated soluble polymers, as well as pH-sensitive nanogels and nondegradable nanogels were obtained (Figure 6). No free, unbound IMDQ could be found in the cross-linked nanogel or non-cross-linked polymers, as determined by the quantitative reversed-phase thin-layer chromatography (RP-TLC) (Figures S34–S36), yet the amount of covalently attached IMDQ was verified by UV–vis spectroscopy and a comparison of the imidazoquinoline absorbance maximum

https://dx.doi.org/10.1021/acs.biomac.0c00205
Biomacromolecules 2020, 21, 2246–2257

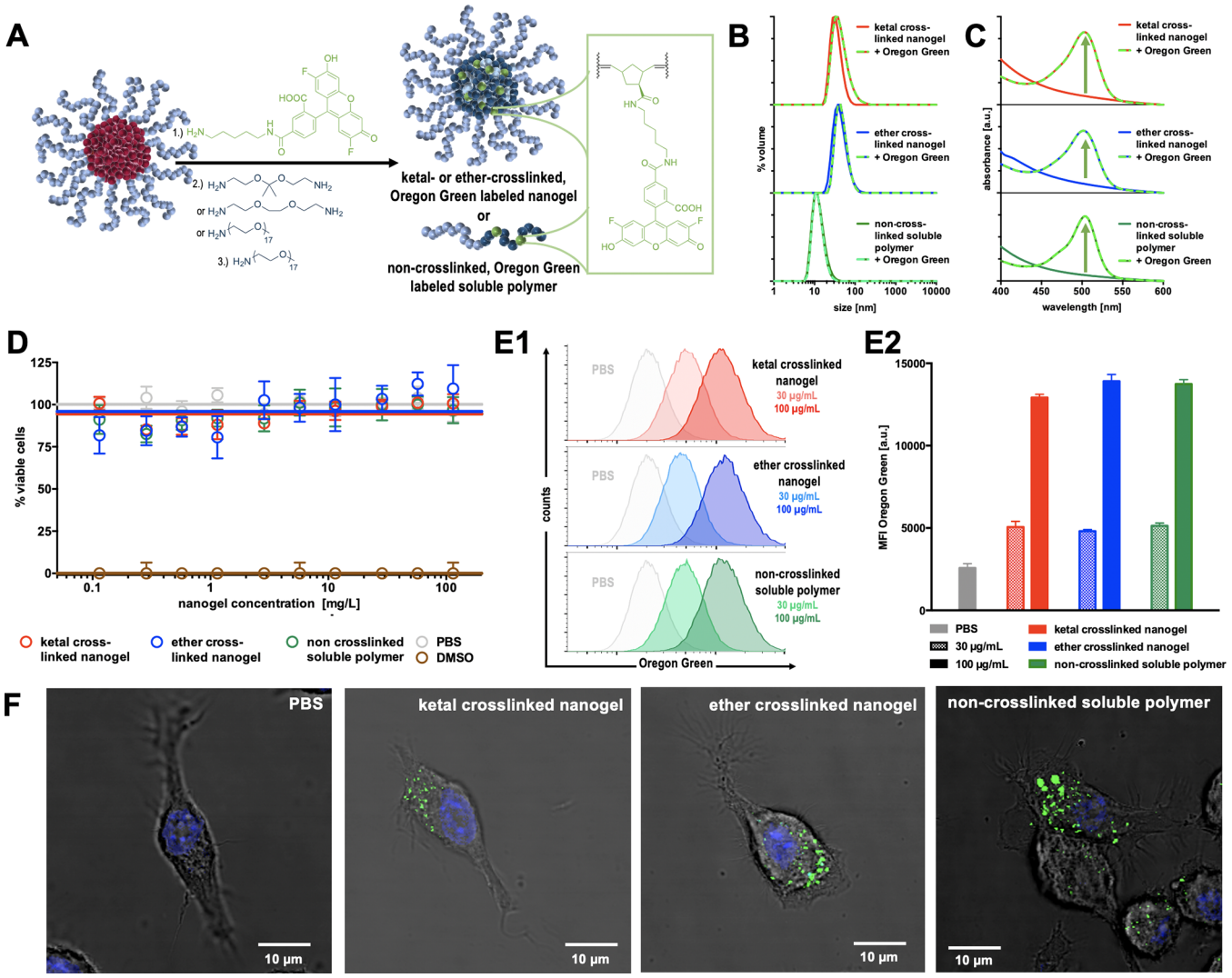

Figure 5. (A) Synthetic scheme for the substitution of Pfp esters in the polymeric precursor micelle cores with Oregon Green cadaverine and different cross-linkers and/or mPEG-amine as hydrophilizing agent. (B) DLS characterization of **poly(Pfp-Nb)$_{50}$-*b*-poly(mPEG-Nb)$_{50}$**-derived cross-linked nanogels and non-cross-linked polymers with and without fluorescent dye. (C) UV absorbance of dye-conjugated nanogels and polymers compared to nonlabeled species. (D) Cell viability assay (MTT) of RAW-Blue macrophages incubated with cross-linked nanogels and non-cross-linked polymers at increasing concentrations for 18 h (n = 4). (E) Flow cytometry histograms (1) and mean fluorescence intensities (MFI) (2) of RAW-Blue macrophages incubated with Oregon Green labeled cross-linked nanogels and non-cross-linked polymers at 30 mg/L and 100 μg/mL for 18 h (n = 3). (F) Confocal laser scanning fluorescence microscopy images of RAW-Blue macrophages incubated with Oregon Green labeled cross-linked nanogels and non-cross-linked polymers at 100 μg/mL for 24 h (green: Oregon Green labeled polymer or nanogel species; blue: nuclei stained with DAPI; gray: dark field image for cell morphology; scale bar: 10 μm).

around 327 nm allowed the determination of the covalent drug load (Figure 6A; detailed information can be found in Supporting Information Figure S37 and Table S1). About 3−4 wt % drug load could be quantified for all species. Interestingly, covalent drug load did not have any significant impact on particle size and distribution of the ketal- or ether-cross-linked nanogels (Figure 6B and S38). Only the non-cross-linked soluble polymer chains tend again to self-assemble in water after IMDQ conjugation, which is probably due to the slight decrease in hydrophilicity caused by the ligated imidazoquinoline (Figures 6B and S38). Nonetheless, for the ketal-cross-linked nanogels, degradation was still confirmed upon exposure to acidic media, as similar size distributions were obtained for the non-cross-linked IMDQ-conjugated polymers (Figure S39).

To test the ability for TLR activation, RAW-Blue macrophages were finally incubated with the prepared IMDQ-loaded particles for 18 h and then characterized. As previously stated, all RAW-Blue macrophages exhibit chromosomal integration of the secreted embryonic alkaline phosphatase reporter construct, which is induced by NF-kB and AP-1. The activation of TLR-7/8 by IMDQ leads to the activation of the downstream signaling cascade and eventually to the release of NF-kB. The secretion of the alkaline phosphatase in turn is utilized for the spectrometric quantification of TLR activation. During these experiments, a decrease in cellular viability could be found for neither the empty nanogels and polymers nor the IMDQ drug species, as characterized by the MTT assay simultaneously (Figure S40).

A readout of the cell culture supernatant media revealed a similar dose-dependent activation of TLR for nondegradable

https://dx.doi.org/10.1021/acs.biomac.0c00205
Biomacromolecules 2020, 21, 2246−2257

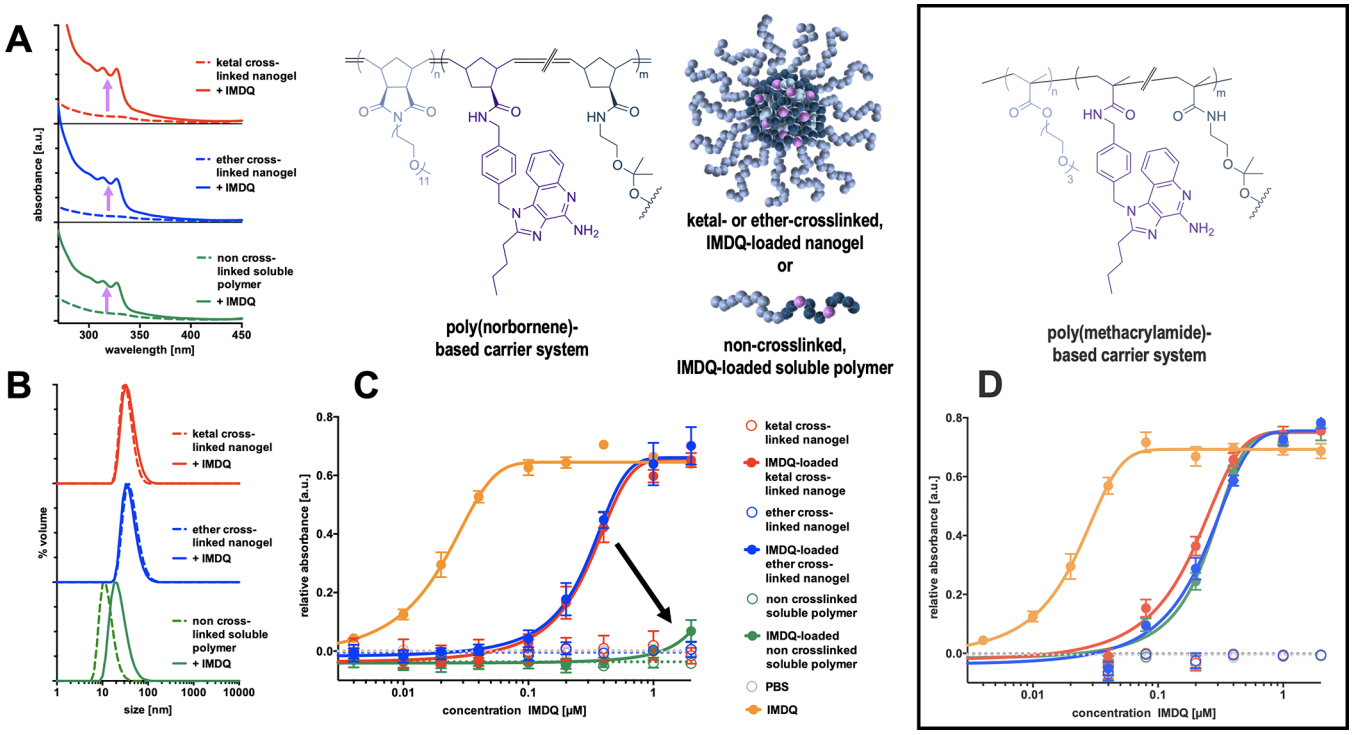

Figure 6. (A) UV−vis spectra for the determination of covalent IMDQ loading to ketal- and ether-cross-linked nanogels as well as non-cross-linked soluble polymers derived from **poly(Pfp-Nb)$_{50}$-*b*-poly(mPEG-Nb)$_{50}$** precursor micelles. (B) DLS measurements of the IMDQ-loaded nanogels and polymers in PBS, compared to the nonloaded species. (C) Results of the TLR stimulation of RAW-Blue macrophages treated with the poly(norbornene)-derived imidazoquinoline nanocarriers (n = 4). (D) Results of the TLR stimulation assay of poly(methacrylamide) carriers (n = 4).

nanogels and acid-labile, ketal-cross-linked nanogels. While the half-maximal effective concentration (EC_{50}) of the free, nonconjugated IMDQ is around 0.02 μM, the activity of the particle-bound IMDQ is about 1 order of magnitude weaker (0.2 μM) for both acid-labile and nondegradable nanogels (Figure 6C). The decrease of activity in nanoparticulate formulation of the drug is comparable to the decrease observed for the poly(methacrylamide)-based nanogels (Figure 6D). Also, the soluble IMDQ-loaded poly(methacrylamide) polymers show a reasonable activity around 0.2 μM. However, in contrast to these systems, the non-cross-linked, soluble IMDQ-loaded, metathesis-derived poly(norbornene)s do not show any significantly high activity in the cell experiments (Figure 6C, green curve). We speculate on different intracellular trafficking mechanisms for these polymers causing this clinically beneficial effect. Further investigation on the intracellular fate of this polymeric material should provide more insight into this behavior.

To conclude, as the poly(norbornene)-based IMDQ nanogels can be degraded under acidic endosomal pH conditions into non-cross-linked soluble polymers, they are first immunologically active but then fall apart into immunologically silent, soluble polymers. This behavior allows a unique access to both temporal and spatial control over the IMDQ activity. The carriers seem to support IMDQ's TLR7/8 stimulation only in their nanoparticular form. Unwanted systemic activation of the immune system seems to be turned off upon nanogel degradation into soluble polymers. Elimination of soluble polymers from the tumoral tissue and its draining lymph nodes into the blood circulation followed by excretion via the kidneys can further prevent long-term overstimulation of the immune system as well as unfavorable carrier accumulation in the body.[44] Altogether, this may regulate IMDQ's high immune stimulatory potency and facilitate its translatability for cancer immunotherapy.

CONCLUSIONS

In summary, for the first time, the synthetic approach of poly(norbornene)-based, pH-degradable core-cross-linked nanogels is introduced in this study. For this purpose, block copolymers of mPEG- and pentafluorophenyl ester-containing poly(norbornene)s could be synthesized with a fast initiating Grubbs catalyst (third generation). The phase separation behavior of the fluorinated reactive ester block in DMSO resulted in reactive micellar particles of adjustable sizes according to the molecular weight and block ratio of the underlying precursor block copolymers.

The reactive ester core-containing micelles were utilized for cross-linking with hydrophilic, pH-sensitive ketal-containing bisamines or a nondegradable ether bisamines instead. Alternatively, non-cross-linked, fully water-soluble species were obtained by treatment with short oligo mPEG amines. However, the degradation of the cross-linked nanogels into soluble polymeric chains was only observed under endosomal pH conditions for the ketal-cross-linked species.

Moreover, the active esters inside the micelle core could further be used for conjugation of fluorescent tracer molecules (for studying cell uptake by flow cytometry and confocal laser scanning fluorescence microscopy) or the highly immune stimulatory small-molecule imidazoquinoline TLR agonist. All carriers exhibited only very low toxicity during cell viability assays. Yet, the immune-modulating activity of drug-conjugated carriers was tested in vitro with RAW-Blue

https://dx.doi.org/10.1021/acs.biomac.0c00205
Biomacromolecules 2020, 21, 2246−2257

macrophages. Interestingly, the activity of IMDQ-conjugated non-cross-linked polymers was decreased drastically, in contrast to nanoparticulate IMDQ. As also acid-degradable ketal particles were designed that fall apart into single polymers, these systems would enable beyond spatial also a temporal control over the immune-modulating activity of IMDQ and, thus, provide access to novel safe and controllable polymeric delivery strategies for such highly potent and promising drugs in cancer immunotherapy.

■ ASSOCIATED CONTENT

Supporting Information

The Supporting Information is available free of charge at https://pubs.acs.org/doi/10.1021/acs.biomac.0c00205.

Purification of *exo*-norbornene-5-carboxylic acid from an exo/endo mixture; MALDI-ToF analysis of the poly-(mPEG-Nb)$_{50}$-homopolymer; SEC traces of the prepared polymers; DOSY measurement; nanogel characterization; TEM measurements; nanogel stability and degradation potential under neutral (extracellular) and acidic (endosomal) pH conditions; and nanogels for immune stimulatory experiments (PDF)

■ AUTHOR INFORMATION

Corresponding Author

Lutz Nuhn − *Max Planck Institute for Polymer Research, 55128 Mainz, Germany;* orcid.org/0000-0003-0761-1106; Phone: +49 (0) 6131-379-311; Email: lutz.nuhn@mpip-mainz.mpg.de

Authors

Johannes Kockelmann − *Max Planck Institute for Polymer Research, 55128 Mainz, Germany*

Judith Stickdorn − *Max Planck Institute for Polymer Research, 55128 Mainz, Germany*

Sabah Kasmi − *Department of Pharmaceutics, Ghent University, 9000 Ghent, Belgium*

Jana De Vrieze − *Department of Pharmaceutics, Ghent University, 9000 Ghent, Belgium*

Michaela Pieszka − *Max Planck Institute for Polymer Research, 55128 Mainz, Germany*

David Yuen W. Ng − *Max Planck Institute for Polymer Research, 55128 Mainz, Germany;* orcid.org/0000-0002-0302-0678

Sunil A. David − *Department of Medicinal Chemistry, University of Minnesota, Minneapolis, Minnesota 55455, United States*

Bruno G. De Geest − *Department of Pharmaceutics, Ghent University, 9000 Ghent, Belgium;* orcid.org/0000-0001-9826-6170

Complete contact information is available at: https://pubs.acs.org/10.1021/acs.biomac.0c00205

Author Contributions

The manuscript was written through contributions of all authors. All authors have given approval to the final version of the manuscript.

Notes

The authors declare no competing financial interest.

■ ACKNOWLEDGMENTS

L.N. kindly acknowledges financial support by the DFG through the Emmy-Noether program and the SFB 1066 Project B04. Moreover, Hans Joachim Räder is gratefully acknowledged for MALDI-ToF MS measurements and Yingke Wu for recording TEM images. The authors also thank the IMB Core Facility Microscopy at the Institute of Molecular Biology (IMB) for their support.

■ REFERENCES

(1) Lybaert, L.; Vermaelen, K.; De Geest, B. G.; Nuhn, L. Immunoengineering through cancer vaccines - a personalized and multi-step vaccine approach towards precise cancer immunity. *J. Controlled Release* **2018**, *289*, 125−145.

(2) Coussens, L. M.; Zitvogel, L.; Palucka, A. K. Neutralizing tumor-promoting chronic inflammation: a magic bullet? *Science* **2013**, *339*, 286−291.

(3) Yu, H.; Tian, Y.; Wang, Y.; Mineishi, S.; Zhang, Y. Dendritic cell regulation of graft-vs.-host disease: immunostimulation and tolerance. *Front. Immunol.* **2019**, *10*, No. 93.

(4) Sprooten, J.; Ceusters, J.; Coosemans, A.; Agostinis, P.; Vleeschouwer, S.; de Zitvogel, L.; Kroemer, G.; Galluzzi, L.; Garg, A. D. Trial watch: dendritic cell vaccination for cancer immunotherapy. *Oncoimmunology* **2019**, *8*, No. e1638212.

(5) Galon, J.; Bruni, D. Approaches to treat immune hot, altered and cold tumours with combination immunotherapies. *Nat. Rev. Drug Discovery* **2019**, *18*, 197−218.

(6) Smith, M.; García-Martínez, E.; Pitter, M. R.; Fucikova, J.; Spisek, R.; Zitvogel, L.; Kroemer, G.; Galluzzi, L. Trial watch: toll-like receptor agonists in cancer immunotherapy. *Oncoimmunology* **2018**, *7*, No. e1526250.

(7) Hammerich, L.; Bhardwaj, N.; Kohrt, H. E.; Brody, J. D. In situ vaccination for the treatment of cancer. *Immunotherapy* **2016**, *8*, 315−330.

(8) Coffman, R. L.; Sher, A.; Seder, R. A. Vaccine adjuvants: putting innate immunity to work. *Immunity* **2010**, *33*, 492−503.

(9) Narayan, R.; Nguyen, H.; Bentow, J. J.; Moy, L.; Lee, D. K.; Greger, S.; Haskell, J.; Vanchinathan, V.; Chang, P.-L.; Tsui, S.; Konishi, T.; Comin-Anduix, B.; Dauphine, C.; Vargas, H. I.; Economou, J. S.; Ribas, A.; Bruhn, K. W.; Craft, N. Immunomodulation by imiquimod in patients with high-risk primary melanoma. *J. Invest. Dermatol.* **2012**, *132*, 163−169.

(10) Harrison, L. I.; Astry, C.; Kumar, S.; Yunis, C. Pharmacokinetics of 852A, an imidazoquinoline Toll-like receptor 7-specific agonist, following intravenous, subcutaneous, and oral administrations in humans. *J. Clin. Pharmacol.* **2007**, *47*, 962−969.

(11) Nuhn, L.; De Koker, S.; Van Lint, S.; Zhong, Z.; Catani, J. P.; Combes, F.; Deswarte, K.; Li, Y.; Lambrecht, B. N.; Lienenklaus, S.; Sanders, N. N.; David, S. A.; Tavernier, J.; De Geest, B. G. Nanoparticle-conjugate TLR7/8 agonist localized immunotherapy provokes safe antitumoral responses. *Adv. Mater.* **2018**, *30*, No. 1803397.

(12) Nuhn, L.; Vanparijs, N.; Beuckelaer, A.; de Lybaert, L.; Verstraete, G.; Deswarte, K.; Lienenklaus, S.; Shukla, N. M.; Salyer, A. C. D.; Lambrecht, B. N.; Grooten, J.; David, S. A.; De Koker, S.; De Geeest, B. G. PH-degradable imidazoquinoline-ligated nanogels for lymph node-focused immune activation. *Proc. Natl. Acad. Sci. U.S.A.* **2016**, *113*, 8098−8103.

(13) Griffith, A. D.; Zaidi, A. K.; Pietro, A.; Hadiono, M.; Yang, J. S.; Davis, R.; Popkin, D. L. A requirement for slc15a4 in imiquimod-induced systemic inflammation and psoriasiform inflammation in mice. *Sci. Rep.* **2018**, *8*, No. 14451.

(14) De Vrieze, J.; Louage, B.; Deswarte, K.; Zhong, Z.; De Coen, R.; Van Herck, S.; Nuhn, L.; Kaas Frich, C.; Zelikin, A. N.; Lienenklaus, S.; Sanders, N. N.; Lambrecht, B. N.; David, S. A.; De Geest, B. G. Potent lymphatic translocation and spatial control over innate immune activation by polymer-lipid amphiphile conjugates of

small-molecule TLR7/8 agonists. *Angew. Chem., Int. Ed.* **2019**, *58*, 15390−15395.
(15) Jewell, C. M.; López, S. C. B.; Irvine, D. J. In situ engineering of the lymph node microenvironment via intranodal injection of adjuvant-releasing polymer particles. *Proc. Natl. Acad. Sci. U.S.A.* **2011**, *108*, 15745−15750.
(16) Liu, H.; Moynihan, K. D.; Zheng, Y.; Szeto, G. L.; Li, A. V.; Huang, B.; van Egeren, D. S.; Park, C.; Irvine, D. J. Structure-based programming of lymph-node targeting in molecular vaccines. *Nature* **2014**, *507*, 519−522.
(17) Moon, J. J.; Suh, H.; Bershteyn, A.; Stephan, M. T.; Liu, H.; Huang, B.; Sohail, M.; Luo, S.; Um, S. H.; Khant, H.; Goodwin, J. T.; Ramos, J.; Chiu, W.; Irvine, D. J. Interbilayer-crosslinked multilamellar vesicles as synthetic vaccines for potent humoral and cellular immune responses. *Nat. Mater.* **2011**, *10*, 243−251.
(18) Nembrini, C.; Stano, A.; Dane, K. Y.; Ballester, M.; van der Vlies, A. J.; Marsland, B. J.; Swartz, M. A.; Hubbell, J. A. Nanoparticle conjugation of antigen enhances cytotoxic T-cell responses in pulmonary vaccination. *Proc. Natl. Acad. Sci. U.S.A.* **2011**, *108*, E989−97.
(19) Reddy, S. T.; van der Vlies, A. J.; Simeoni, E.; Angeli, V.; Randolph, G. J.; O'Neil, C. P.; Lee, L. K.; Swartz, M. A.; Hubbell, J. A. Exploiting lymphatic transport and complement activation in nanoparticle vaccines. *Nat. Biotechnol.* **2007**, *25*, 1159−1164.
(20) Lynn, G. M.; Laga, R.; Darrah, P. A.; Ishizuka, A. S.; Balaci, A. J.; Dulcey, A. E.; Pechar, M.; Pola, R.; Gerner, M. Y.; Yamamoto, A.; Buechler, C. R.; Quinn, K. M.; Smelkinson, M. G.; Vanek, O.; Cawood, R.; Hills, T.; Vasalatiy, O.; Kastenmüller, K.; Francica, J. R.; Stutts, L.; Tom, J. K.; Ryu, K. A.; Esser-Kahn, A. P.; Etrych, T.; Fisher, K. D.; Seymour, L. W.; Seder, R. A. In vivo characterization of the physicochemical properties of polymer-linked TLR agonists that enhance vaccine immunogenicity. *Nat. Biotechnol.* **2015**, *33*, 1201−1210.
(21) Nuhn, L.; van Hoecke, L.; Deswarte, K.; Schepens, B.; Li, Y.; Lambrecht, B. N.; de Koker, S.; David, S. A.; Saelens, X.; De Geest, B. G. Potent anti-viral vaccine adjuvant based on pH-degradable nanogels with covalently linked small molecule imidazoquinoline TLR7/8 agonist. *Biomaterials* **2018**, *178*, 643−651.
(22) Stickdorn, J.; Nuhn, L. Reactive-ester derived polymer nanogels for cancer immunotherapy. *Eur. Polym. J.* **2020**, *124*, No. 109481.
(23) Nuhn, L.; van Herck, S.; Best, A.; Deswarte, K.; Kokkinopoulou, M.; Lieberwirth, I.; Koynov, K.; Lambrecht, B. N.; De Geest, B. G. FRET Monitoring of Intracellular Ketal Hydrolysis in Synthetic Nanoparticles. *Angew. Chem., Int. Ed.* **2018**, *57*, 10760−10764.
(24) Leber, N.; Kaps, L.; Aslam, M.; Schupp, J.; Brose, A.; Schäffel, D.; Fischer, K.; Diken, M.; Strand, D.; Koynov, K.; Tuettenberg, A.; Nuhn, L.; Zentel, R.; Schuppan, D. SiRNA-mediated in vivo gene knockdown by acid-degradable cationic nanohydrogel particles. *J. Controlled Release* **2017**, *248*, 10−23.
(25) Choi, T.-L.; Grubbs, R. H. Controlled living ring-opening-metathesis polymerization by a fast-initiating ruthenium catalyst. *Angew. Chem., Int. Ed.* **2003**, *42*, 1743−1746.
(26) Matson, J. B.; Grubbs, R. H. Synthesis of fluorine-18 functionalized nanoparticles for use as in vivo molecular imaging agents. *J. Am. Chem. Soc.* **2008**, *130*, 6731−6733.
(27) Roloff, A.; Nelles, D. A.; Thompson, M. P.; Yeo, G. W.; Gianneschi, N. C. Self-Transfecting Micellar RNA: Modulating Nanoparticle Cell Interactions via High Density Display of Small Molecule Ligands on Micelle Coronas. *Bioconjugate Chem.* **2018**, *29*, 126−135.
(28) Nuhn, L.; Hirsch, M.; Krieg, B.; Koynov, K.; Fischer, K.; Schmidt, M.; Helm, M.; Zentel, R. Cationic nanohydrogel particles as potential siRNA carriers for cellular delivery. *ACS Nano* **2012**, *6*, 2198−2214.
(29) Leber, N.; Nuhn, L.; Zentel, R. Cationic Nanohydrogel Particles for Therapeutic Oligonucleotide Delivery. *Macromol. Biosci.* **2017**, *17*, No. 1700092.
(30) Das, A.; Theato, P. Activated Ester Containing Polymers: Opportunities and Challenges for the Design of Functional Macromolecules. *Chem. Rev.* **2016**, *116*, 1434−1495.
(31) Shukla, N. M.; Malladi, S. S.; Mutz, C. A.; Balakrishna, R.; David, S. A. Structure-activity relationships in human toll-like receptor 7-active imidazoquinoline analogues. *J. Med. Chem.* **2010**, *53*, 4450−4465.
(32) Veccharelli, K. M.; Tong, V. K.; Young, J. L.; Yang, J.; Gianneschi, N. C. Dual responsive polymeric nanoparticles prepared by direct functionalization of polylactic acid-based polymers via graft-from ring opening metathesis polymerization. *Chem. Commun.* **2016**, *52*, 567−570.
(33) Zhang, K.; Lackey, M. A.; Wu, Y.; Tew, G. N. Universal cyclic polymer templates. *J. Am. Chem. Soc.* **2011**, *133*, 6906−6909.
(34) Gref, R.; Minamitake, Y.; Peracchia, M. T.; Trubetskoy, V.; Torchilin, V.; Langer, R. Biodegradable long-circulating polymeric nanospheres. *Science* **1994**, *263*, 1600−1603.
(35) Torchilin, V. P.; Klibanov, A. L.; Huang, L.; O'Donnell, S.; Nossiff, N. D.; Khaw, B. A. Targeted accumulation of polyethylene glycol-coated immunoliposomes in infarcted rabbit myocardium. *FASEB J.* **1992**, *6*, 2716−2719.
(36) Knop, K.; Hoogenboom, R.; Fischer, D.; Schubert, U. S. Poly(ethylene glycol) in drug delivery: pros and cons as well as potential alternatives. *Angew. Chem., Int. Ed.* **2010**, *49*, 6288−6308.
(37) Kanaoka, S.; Grubbs, R. H. Synthesis of Block Copolymers of Silicon-Containing Norbornene Derivatives via Living Ring-Opening Metathesis Polymerization Catalyzed by a Ruthenium Carbene Complex. *Macromolecules* **1995**, *28*, 4707−4713.
(38) Larroche, C.; Laval, J. P.; Lattes, A.; Basset, J. M. Ring-opening polymerization of norbornene substituted with amine and ammonium groups. *J. Org. Chem.* **1984**, *49*, 1886−1890.
(39) Wolfe, P. S.; Wagener, K. B. Investigation of Organoboronates in Metathesis Polymerization. *Macromolecules* **1999**, *32*, 7961−7967.
(40) Wolf, W. J.; Lin, T.-P.; Grubbs, R. H. Examining the Effects of Monomer and Catalyst Structure on the Mechanism of Ruthenium-Catalyzed Ring-Opening Metathesis Polymerization. *J. Am. Chem. Soc.* **2019**, *141*, 17796−17808.
(41) Neises, B.; Steglich, W. Simple Method for the Esterification of Carboxylic Acids. *Angew. Chem., Int. Ed.* **1978**, *17*, 522−524.
(42) Vogel, N.; Théato, P. Controlled Synthesis of Reactive Polymeric Architectures Using 5-Norbornene-2-carboxylic Acid Pentafluorophenyl Ester. *Macromol. Symp.* **2007**, *249*−*250*, 383−391.
(43) Forcina, V.; García-Domínguez, A.; Lloyd-Jones, G. C. Kinetics of initiation of the third generation Grubbs metathesis catalyst: convergent associative and dissociative pathways. *Faraday Discuss.* **2019**, *220*, 179−195.
(44) Fox, M. E.; Szoka, F. C.; Fréchet, J. M. J. Soluble polymer carriers for the treatment of cancer: the importance of molecular architecture. *Acc. Chem. Res.* **2009**, *42*, 1141−1151.

https://dx.doi.org/10.1021/acs.biomac.0c00205
Biomacromolecules 2020, 21, 2246−2257